HHS Public Access

Author manuscript

Ann Biomed Eng. Author manuscript; available in PMC 2022 September 01.

Published in final edited form as:

Ann Biomed Eng. 2021 September ; 49(9): 2114–2125. doi:10.1007/s10439-021-02736-9.

Effect of 3D Printing Temperature on Bioactivity of Bone Morphogenetic Protein-2 Released from Polymeric Constructs

Gerry L. Koons, BS[a,b,c], **Panayiotis D. Kontoyiannis**[d], **Mani Diba, PhD**[a], **Letitia K. Chim, MSE**[a], **David W. Scott, PhD**[e], **Antonios G. Mikos, PhD**[a,b,*]

[a]Department of Bioengineering, Rice University, Houston, TX, USA

[b]Center for Engineering Complex Tissues, USA

[c]Medical Scientist Training Program, Baylor College of Medicine, Houston, TX, USA

[d]Department of Biochemistry and Cell Biology, Rice University, Houston, TX, USA

[e]Department of Statistics, Rice University, Houston, TX, USA

Abstract

Growth factors such as bone morphogenetic protein-2 (BMP-2) are potent tools for tissue engineering. Three-dimensional (3D) printing offers a potential strategy for delivery of BMP-2 from polymeric constructs; however, these biomolecules are sensitive to inactivation by the elevated temperatures commonly employed during extrusion-based 3D printing. Therefore, we aimed to correlate printing temperature to the bioactivity of BMP-2 released from 3D printed constructs composed of a model polymer, poly(propylene fumarate). Following encapsulation of BMP-2 in poly(DL-lactic-*co*-glycolic acid) particles, growth factor-loaded fibers were fabricated at three different printing temperatures. Resulting constructs underwent 28 days of aqueous degradation for collection of released BMP-2. Supernatants were then assayed for the presence of bioactive BMP-2 using a cellular assay for alkaline phosphatase activity. Cumulative release profiles indicated that BMP-2 released from constructs that were 3D printed at physiologic and intermediate temperatures exhibited comparable total amounts of bioactive BMP-2 release as those encapsulated in non-printed particulate delivery vehicles. Meanwhile, the elevated printing temperature of 90 ºC resulted in a decreased amount of total bioactive BMP-2 release from the fibers. These findings elucidate the effects of elevated printing temperatures on BMP-2 bioactivity during extrusion-based 3D printing, and enlighten polymeric material selection for 3D printing with growth factors.

Keywords

3D printing; growth factor; protein delivery; tissue engineering; biomaterials

[*]Corresponding author: Antonios G. Mikos, PhD, BioScience Research Collaborative, Department of Bioengineering, MS-142, 6500 Main Street, Houston, TX 77030, USA, Telephone: (713) 348-5355, Fax: (713) 348-4244, mikos@rice.edu.

Introduction

For biomedical applications ranging from regenerative medicine and wound healing to potential therapies for ischemic cardiac and neurologic conditions, the controlled delivery of therapeutic proteins such as growth factors bears great potential for directing cellular activities biomimetically[55, 57]. These biomolecules can be incorporated into and delivered from constructs composed of biomaterials, particularly synthetic polymers with tunable material properties such as their degradation rate[3, 40]. Effective incorporation of growth factors into a polymeric matrix can prevent immediate diffusion of large quantities of the loaded biomolecule from its biomaterial carrier[26, 28, 35]. This strategy aims to avoid excessive burst release and a consequent need to load supraphysiologic dosages to compensate for this early loss.

However, growth factor bioactivity can be debilitated by conditions employed during fabrication of biomaterial constructs[26]. For example, extrusion-based three-dimensional (3D) printing is an increasingly accessible and cost-effective fabrication method with the capacity for enabling complex spatial patterning of growth factors, in order to target desired cell populations and establish directionality of resulting tissue growth[2, 38]. To lower a material's viscosity sufficiently to allow extrusion, some biomaterials must be heated to temperatures incompatible with the maintenance of growth factor bioactivity[17, 54]. While less mechanically robust hydrogels can be 3D printed by extrusion-based techniques at or below physiologic temperatures[45, 58], hydrophobic and synthetic polymeric biomaterials possessing the mechanical properties needed for applications like bone tissue engineering must often be subjected to elevated printing temperatures[18, 25]. The introduction of this additional thermal energy may disrupt the molecular interactions that dictate the characteristic 3D conformation of loaded growth factors[11, 13]. These biomolecules may then become denatured, rendered unrecognizable to the membrane receptors on targeted cells, and are thus irreversibly inactivated[7, 41].

To avoid this inactivation of growth factors during extrusion-based 3D printing with mechanically robust materials, previous studies have altered various components of biomaterial printing formulations. For example, in one strategy, biomaterial formulations are prepared by supplementing a polymer with its constituent monomer, to reduce formulation viscosity and enable printing at lower temperatures, while maintaining other material characteristics[50]. In another strategy, the biomolecules are encapsulated in intermediary delivery vehicles composed of materials with reduced heat conduction, to provide a protective barrier from the elevated temperature of the bulk polymer matrix during printing[46]. While this prior work has demonstrated preservation of growth factor bioactivity using these strategies[31, 46], retention of the bioactivity of growth factors at different 3D printing temperatures has not yet been investigated systematically. Moreover, the method of particulate delivery vehicle fabrication must also permit maintenance of growth factor bioactivity, such as during double emulsion particle synthesis techniques with potential exposure of the growth factor to a denaturing interface with the strong organic solvent[8].

Importantly, altering biomaterial formulations and printing temperatures for the purpose of growth factor bioactivity retention may also affect biomaterial characteristics such as

crosslinking behavior[29, 33, 49]. Therefore, the modification of these fabrication parameters may in turn alter the kinetics of growth factor release[16, 39]. This influence could necessitate further optimization of biomaterial formulations for 3D printing, such that possible printing temperatures allow for both the preservation of growth factor bioactivity and a growth factor delivery rate that is advantageous for interacting with cells at key timepoints during therapeutic processes[14].

In the present work, we investigated the effect of printing temperature on the release of bioactive growth factors from 3D printed polymeric constructs. Specifically, we employed the synthetic polymer poly(propylene fumarate) (PPF) supplemented with its monomer, diethyl fumarate (DEF), as a model biomaterial formulation. Bone morphogenetic protein-2 (BMP-2), an osteogenic growth factor used for bone tissue engineering, was encapsulated in particulate delivery vehicles made of poly(DL-lactic-*co*-glycolic acid) (PLGA), and these particles were mixed with PPF and DEF prior to extrusion-based 3D printing at physiologic (37 °C), intermediate (60 °C), and elevated (90 °C) temperatures. Resulting biomaterial fibers were evaluated morphologically and subjected to degradation and release studies to collect released BMP-2. The release kinetics of bioactive BMP-2, as determined by the upregulation of cellular alkaline phosphatase (ALP) enzyme production, were characterized to elucidate the possible relationships between 3D printing temperatures and the release of bioactive growth factor from the biomaterial constructs. Figure 1 presents a summary of this experimental process. We hypothesized that while higher printing temperatures would result in lower bioactive BMP-2 release due to thermal denaturation, this effect would be minimized at lower printing temperatures. Consequently, this study enlightens the considerations for selection and design of biomaterial formulations and printing conditions for extrusion-based 3D printing with growth factors.

Materials and Methods

Synthesis of PPF

PPF was synthesized according to the procedure described by Kasper *et al.*[19] All reagents were purchased from Sigma-Aldrich Corporation (St. Louis, MO) unless otherwise stated. Briefly, DEF was reacted with propylene glycol (Fisher Scientific™; Waltham, MA) in a 1:3 molar ratio at 130 °C, under mechanical stirring and nitrogen flow. After allowing this reaction to proceed for 32 hr, the transesterification reaction was performed under high vacuum for 6 hr to synthesize PPF. The resulting product was then purified with five different aqueous washes and an ether wash to remove remaining unreacted components. The final number-average molecular weight (M_n) and weight-average molecular weight (M_w) of purified PPF were measured by an ACQUITY advanced polymer chromatography™ (APC) system (Waters™ Corporation; Milford, MA) as the averaged values for six injections with reference to polystyrene standards.

Synthesis of BMP-2–loaded PLGA particles

Growth factor-loaded PLGA particles were synthesized using a modified water-in-oil-in-water double emulsion solvent evaporation technique[20, 43], as described in Supplementary Methods.

Extrusion-based 3D printing of PLGA particle–loaded PPF-based fibers

To prepare the mixture for printing, DEF was added to the synthesized PPF polymer in a 90:10 PPF:DEF mass ratio. In addition to participating in the post-extrusion photocrosslinking reaction, the DEF monomer was included to lower the temperatures required for the printing process by reducing the viscosity of the printing formulation[22, 50]. The photoinitiator bisacylphosphine oxide (BAPO; Sigma-Aldrich Corporation; St. Louis, MO) was then introduced to the mixture at 1 wt% concentration to enable photocrosslinking. The components were next homogeneously mixed at 100 °C using a magnetic stirrer, then allowed to cool to room temperature[50]. The mixture was subsequently warmed to 37 °C, and 2 wt% of unloaded or BMP-2–loaded PLGA particles were mixed in using a spatula. This mass concentration was determined to be the maximum loading of PLGA particles for this printing formulation (the synthesized PPF with 10 wt% DEF) that permitted consistently uninterrupted material extrusion during preliminary printing attempts. The mixture was then kept at 37 °C overnight to enable its transfer into a high-temperature printing cartridge with a 22G needle.

For printing, the cartridges were inserted into high-temperature printing heads of an extrusion-based 3D-Bioplotter® (EnvisionTEC; Gladbeck, Germany). The printing heads were heated to physiologic, intermediate, or elevated temperatures (37, 60, or 90 °C, respectively) for at least 30 min prior to printing, and the printing platform was cooled to 10 °C. Thereafter, the materials were extruded onto glass slides in a single-layer rectangular pattern at printing pressures and speeds adjusted to minimize differences in fiber diameter for the different printing temperatures (Table 1). Upon completion of printing, the fibers were subjected to 1000 consecutive flashes (at a rate of 10 flashes/s for a total duration of 100 s) within a multi-lamp flash box of 200 W power and 300-700 nm spectral distribution (Otoflash Post Curing Light Pulsing Unit, EnvisionTEC; Gladbeck, Germany). The printed constructs were positioned approximately 4.2 cm from the light source, and the flashes were administered in increments of 100 flashes followed by 1 min of flash cessation to minimize heating of the printed fibers due to high-energy light flashes.

Morphological characterization of PLGA particles and 3D printed fibers

Morphological characteristics of particles and printed fibers were analyzed using scanning electron microscopy (SEM). To this end, PLGA particles or 3D printed PPF-based fibers were distributed on carbon tape and sputter-coated with a 10 nm gold layer prior to imaging with a Quanta 400 field emission gun ESEM (Field Electron and Ion Company; Hillsboro, OR). Particle size was measured through manual analysis using ImageJ by overlaying a 7 x 8 grid onto the image. The boxes (fifty-six in total) delineated by the gridlines were each assigned a sequential number, and a numerical randomization algorithm was employed to select five of the boxes. The diameters of all particles positioned fully or partially within the chosen grid boxes were measured, resulting in 184 distinct particles' diameters measured through this process. Finally, optical images were acquired using a trinocular stereomicroscope (SM-4TZ-144A, AmScope; Irvine, CA) from 10 fibers with or without unloaded PLGA particles per printing temperature, and pre-degradation fiber diameters were manually quantified using ImageJ.

Degradation of 3D printed fibers in aqueous medium

Fibers printed with or without unloaded PLGA particles were subjected to 28 days of aqueous degradation conditions with measurements of supernatant pH, pre- and post-degradation fiber diameters, and sample mass loss, as noted in Supplementary Methods.

Collection of BMP-2 released from 3D printed PPF-based fibers

$n = 4$ samples of fibers with BMP-2–loaded PLGA particles were fabricated per printing temperature. The printed fibers were sterilized by ethylene oxide with an Anprolene AN74i gas sterilizer (Andersen Sterilizers; Haw River, NC), and 4-(2-hydroxyethyl)-1-piperazineethanesulfonic (HEPES) buffer solution was introduced at a concentration of 150 mg printed fibers or 3 mg BMP-2–loaded PLGA particle controls per mL buffer solution.

During the 28-day study, the release supernatant was collected and replaced at each timepoint on days 1, 4, 7, 10, 14, 18, 21, 24, and 28. Maximum removal of supernatant was facilitated by centrifuging the tubes containing release samples at 1600 x g for 5 min for particle samples, or 400 x g for 2 min for fiber samples. Upon collection, a 450 μL aliquot of each release supernatant was prepared for the bioactivity assay by adding a 7 mg mixture of high-glucose Dulbecco's Modified Eagle Medium (DMEM; Thermo Fisher Scientific; Waltham, MA) and sodium bicarbonate (Sigma-Aldrich Corporation; St. Louis, MO) in a 7.3:1 DMEM:bicarbonate mass ratio, along with 45 μL of fetal bovine serum (FBS; 10% of total aliquot volume, Gemini Bio; West Sacramento, CA) and 4.5 μL of penicillin-streptomycin (1% of total aliquot volume). All release samples were then stored at −80 °C until the bioactivity assays were performed.

Bioactivity of released BMP-2

Collected release supernatants were exposed to the BMP-2–responsive murine bone marrow stromal W-20-17 cell line, which was then assayed for ALP activity normalized to DNA content. These measurements were compared to normalized ALP activity values stimulated by known concentrations of bioactive BMP-2, in order to calculate cumulative release profiles of bioactive growth factor for each experimental group. A detailed description of this methodology can be found in Supplementary Methods.

Statistical analysis

GraphPad Prism software was used to perform the statistical analyses with a two-way analysis of variance with repeated measures and *post hoc* Tukey's honestly significant difference test to compare values among experimental groups and release timepoints. Unpaired t-tests with Bonferroni-Dunn correction were performed to compare measured values to the baseline for the culture medium control without added growth factor (0 ng/mL BMP-2) for the bioactivity study data. Data are presented as mean ± standard deviation, with a statistical significance threshold of $p < 0.05$.

Results

Morphological properties and degradation behavior of PLGA particles and 3D printed fibers

PPF was successfully synthesized with a measured M_n of 2891 Da and M_w of 4068 Da. The PLGA particle synthesis yielded 356 mg of BMP-2–loaded PLGA particles with a theoretical loading of approximately 0.7 μg of BMP-2 per mg of PLGA particles (assuming 100% loading efficiency). The average diameter of synthesized particles was 980 ± 1426 nm (Fig. 2A). These materials were mixed and printed at 37, 60, or 90 °C, with average fiber diameters of 0.831 ± 0.179, 1.093 ± 0.259, and 1.387 ± 0.218 mm, respectively (Fig. 2B). PPF-based fibers without incorporated PLGA particles were also fabricated with average diameters of 0.916 ± 0.049, 0.923 ± 0.270, and 0.851 ± 0.102 mm upon printing at 37, 60, or 90 °C, respectively.

These fibers were then subjected to 28 days of incubation in aqueous medium, with measurement of pH and replacement of the medium every 3-4 days after the Day 1 timepoint. Figure 3A illustrates the changes of pH for the degradation buffer over 28 days. All printed fiber groups exhibited significantly reduced pH relative to the PLGA particle group for Days 1-18 (Supplementary Table S1). In addition, the particle-containing fiber groups printed at 37 °C for Day 24, or at 37 and 60 °C for Day 28, showed significantly reduced pH relative to the PLGA particle group.

Furthermore, as shown in Figure 3B, none of the groups exhibited a significant change in fiber diameter after exposure to 28 days of degradation conditions. Fibers with the highest printing temperature (90 °C) were larger than those fabricated at lower printing temperatures both before and after degradation. Moreover, higher mass loss (Fig. 3C) was generally observed for printed fibers without PLGA particles (9.1 ± 2.4 %, 7.6 ± 1.7 %, and 5.0 ± 0.3 % for printing temperatures of 37, 60, or 90 °C, respectively) than for particle-loaded fibers (3.4 ± 2.7 %, 6.0 ± 0.2 %, and 5.0 ± 1.1 %, respectively), although most of these comparisons were not statistically significant. While the non-particle-containing 90 °C printing temperature group displayed non-zero mass loss despite its slightly increased average fiber diameter after degradation, the latter finding was not statistically significant. Meanwhile, the mass loss of the PLGA particle control samples was undetectable after 28 days of incubation in aqueous medium.

Normalized ALP activity stimulated by bioactive BMP-2 release

Prior to normalization by cellular DNA content, none of the measured ALP activities were significantly elevated from the baseline production of the enzyme as measured from the non-BMP-2 containing control (Supplementary Fig. S1A). Significant differences in ALP activity stimulated by different experimental groups only occurred for Day 1 (Supplementary Table S2a), and within each experimental group, differences in ALP activity occurred between one or two timepoints (Supplementary Table S3a). Meanwhile, all experimental groups were found to yield equal or greater cell numbers than the non-BMP-2-containing control (Supplementary Fig. S1B). For all groups, cells exposed to supernatant samples from earlier release timepoints (such as Day 4 or Day 7) were lower in

number than those exposed to supernatants collected later in the studied release timeframe (Supplementary Table S3b).

The ALP activity normalized by DNA for each experimental group is shown in Figure 4A. Notably, normalized ALP activity for the 37 °C and 60 °C printing temperature groups was higher than that of the 90 °C printing temperature and PLGA particle groups at Day 4 (Supplementary Table S2c). Each printed fiber group also displayed higher normalized ALP values at some of the earlier timepoints (such as Day 1, Day 4, or Day 7) relative to later timepoints (such as Days 21, Day 24, or Day 28; Supplementary Table S3c). Meanwhile, comparisons among release timepoints for the PLGA particle group revealed no significant differences.

Calculated bioactive BMP-2 concentration and cumulative release

Next, the normalized ALP activity stimulated in cells exposed to controls of BMP-2 added to culture medium at known concentrations were used to generate a calibration curve (Fig. 4B). Four-parameter logistic regression was performed to derive an equation for correlating normalized ALP activity to the concentration of bioactive BMP-2 present (0-100 ng/mL), yielding the following parameters: A = 34.39, B = 3.140, C = 2.563, and D = 0.1543 (R^2 = 0.8767; see Supplementary Fig. S2 for a description of parameters). This equation was then employed to calculate the concentration of bioactive BMP-2 present in each release sample from normalized ALP measurements. These calculated values of BMP-2 ranged from 0-64 ng/mL and were then summated to quantify cumulative release of bioactive growth factor from 3D printed fibers and particulate delivery vehicles, as shown in Figure 4C and Supplementary Figure S3. During the first half of the release study (Days 4-14), the cumulative release profiles for both the 37 and 60 °C printing temperatures indicated significantly higher bioactive BMP-2 release than for the 90 °C group (Supplementary Table S2d). A significantly higher amount of bioactive BMP-2 release was also detected for the 60 °C group relative to the PLGA particle-only groups on Days 4-21. By the end of the release study (Days 24-28), the cumulative release of bioactive BMP-2 from PLGA particles became statistically equivalent to that of the 37 and 60 °C groups, while the 90 °C group remained at lower bioactive BMP-2 release than for the 60 °C group.

Discussion

BMP-2–loaded PLGA particles and 3D printed fibers with embedded growth factor-loaded particles were incubated in release medium for 28 days, with supernatant collection and replacement every 3-4 days to avoid growth factor denaturation upon extended presence in aqueous solution[23]. W-20-17 cells, a mouse bone marrow stromal cell line which upregulates expression of ALP enzyme upon exposure to bioactive BMP-2 in a dose-dependent manner, were then cultured in the release supernatants[1, 20]. ALP activity was assessed by colorimetric assay relative to that induced by known values of fresh BMP-2 added to the culture medium as controls[20, 24, 47]. These values were normalized to cell number using a DNA quantification assay[44].

For all experimental groups, upregulation of ALP activity at each individual timepoint was not detected. This lack of increase in ALP activity relative to the cells' baseline

production of this enzyme, as measured from non-BMP-2-exposed cells, is likely due to the necessity to dilute the collected release supernatants substantially (100-fold) before introduction to cells. This dilution was performed in order to minimize the previously reported[12, 34, 48, 53] concentration-dependent *in vitro* cytotoxicity of the employed PPF-based bulk material components and their degradation products. Other investigations demonstrating preserved cell viability with PPF-based systems similarly feature high degrees of material dilution[6, 52, 53]. Additional studies have also shown the sensitivity of this particular cell line to increased concentrations of material additives such as crosslinking agents[24]. The cell number measurements indicate the successful preservation of cell viability at the implemented degree of sample dilution. However, it is possible that bioactive BMP-2 was indeed present in the samples collected at the specified time intervals, yet the growth factor concentrations were then diluted below the detection limit of the BMP-2 bioactivity assay, in order to enable the survival of the growth factor-responsive cells.

Thus, the challenge of incorporating growth factors into 3D printed scaffolds lies not only in the maintenance of their bioactivity, but also in the necessity to verify their bioactivity experimentally through their introduction to cell culture. For such *in vitro* investigations, these biomolecules must be present at sufficiently high concentrations to be detectable, yielding statistically significant effects despite the inherent variability of biological systems. For material systems displaying concentration-dependent cytotoxicity, the loading quantity of growth factor must be additionally increased according to the anticipated dilution factor, to enable detectability by subsequent cellular assays.

The cumulative release of bioactive growth factor was quantified relative to upregulated alkaline phosphatase expression stimulated by known concentrations of unencapsulated BMP-2. While the employed concentrations of these growth factor controls are consistent with previous reports[20, 24], additional intermediary concentrations are suggested for future studies to provide additional datapoints for fitting of the calibration curve using four-parameter logistic regression. In the current work, an early release profile of gradual rather than burst release of bioactive growth factor from the PLGA delivery vehicles was observed, while the two lower-temperature printing groups exhibited bioactive BMP-2 release within the earliest timepoints. These results may be attributed to the significantly decreased pH observed during the Day 1-18 timepoints for degradation of the 3D printed, particle-containing fiber groups (Fig. 3A), as local acidity is known to accelerate the degradation of PLGA[4, 42].

These findings differ from another investigation[31] employing scaffold fabrication by microstereolithography, with the same material components including 30 wt% DEF and a printing temperature of 60 °C. Relatively delayed kinetics of growth factor release from the 3D printed fibers relative to PLGA particles alone were observed, which was attributed to the additional diffusional barrier provided by the PPF-based bulk material. However, it bears consideration that the bulk material might also serve as a diffusional barrier to the degradation products of PLGA, thus facilitating the local accumulation of these acidic compounds and contributing to the auto-catalytic degradation of the polymeric delivery vehicles, with subsequently enhanced release of encapsulated BMP-2 from particle-containing fibers relative to PLGA particles alone[4, 42].

For the present study, warming of PLGA particles within fibers above ambient temperature may have altered their permeability to BMP-2 diffusion, as the glass transition temperature of this PLGA formulation is 44-48 °C. Therefore, for the physiologic and intermediate printing temperature groups (37 and 60 °C), the PPF-based fibers with embedded PLGA particles displayed accelerated growth factor release to a statistically notable extent, while at the final timepoints, no statistically significant difference existed between the total amounts of bioactive BMP-2 released from PLGA particles and these experimental groups. The non-printed particles were consequently revealed to release statistically equivalent quantities of bioactive growth factor at a slower release rate than the two lower printing temperature groups.

While the differences between the 37 °C, 60 °C, and PLGA groups were not statistically significant at the final timepoints, their means displayed a notable trend of increase from the lower values for the PLGA group to the highest values for the 60 °C group. We postulate that the trend of higher and faster release of BMP-2 from fibers printed at 60 °C than from those fabricated at 37 °C could relate to increased PLGA degradation at this transiently elevated printing temperature, with resulting accumulation of acidic polymeric degradation products, auto-catalysis, and increased biomolecule release[56].

In terms of bioactivity, the cumulative release of BMP-2 calculated for Day 4 indicates preservation of growth factor bioactivity for the 37 and 60 °C printing temperatures rather than for 90 °C, with the different release pattern for PLGA resulting in its value being initially less than that of the 60 °C group. Indeed, the presence of bioactive growth factor for the 60 °C group was higher than that of the 90 °C at all timepoints beginning with Day 4, indicating potential inactivation of growth factor bioactivity rather than a delayed release profile. Unlike the eventual release of a statistically equivalent amount of bioactive growth factor from the PLGA particles, the outcome observed for the 90 °C group can be attributed to denaturation of the growth factor at this printing temperature, as other studies have indicated the reduction of *in vitro* BMP-2 bioactivity at 65 or 90 °C using different cell lines[36, 41].

Therefore, printing formulations must be chosen to enable preparation, transfer to the printing cartridge, and extrusion printing at minimized processing temperatures, which can be accomplished by introducing additives such as DEF to decrease material viscosity. In the present study, systematic investigation of various printing temperatures was intended to elucidate selection of other materials for extrusion-based 3D printing with BMP-2, revealing that material formulations should require printing temperatures of less than 90 °C to avoid inactivation of this growth factor. For different growth factors and other temperature-sensitive bioactive molecules, similar consideration must be given to excluding materials or material formulations which require printing temperatures that exceed the biomolecules' tolerance for preserved bioactivity. Furthermore, during each of these experimental processing steps, such as the post-synthesis lyophilization of BMP-2–loaded PLGA particles, and the frozen storage of release supernatants, the sensitivity of growth factor bioactivity to freeze-thawing must be carefully considered and accommodated.

Additionally, material selection for the present study was intended to enable printing of the chosen formulation at 37, 60, and 90 °C with comparable printed fiber diameters, in order to avoid introducing an additional variable (the surface area for material degradation and growth factor release) to the comparison among experimental groups. This objective was attempted by printing the higher-temperature and thus lower-viscosity formulations at lower pressures and higher speeds (Table 1). Nonetheless, increasing printing temperatures yielded larger fiber diameters, likely because the decreased material viscosity compromised the material's ability to maintain its original extruded diameter and morphology (presumably matching that of the printing nozzle), due to material flow that resulted in spreading on the printing surface[9, 27, 30, 51]. As this phenomenon may be influenced by the time delay between extrusion of the liquid material and its solidification via photocrosslinking, the employment of simultaneous photocrosslinking during extrusion through the nozzle can improve the consistency of fiber diameters for different printing temperatures in future studies[15].

For all investigated printing temperatures, these fibers did not undergo a significant decrease in diameter, while displaying less than 10% mass loss upon 28 days of aqueous incubation, indicating the capacity of released growth factor to diffuse through the PPF and PLGA matrices, both of which undergo bulk hydrolytic degradation[5, 37]. The pH changes caused by fiber incubation were also consistent among printed groups and thus did not appear to independently impact bioactivity of the reputedly acid-stable BMP-2 growth factor[32].

When adding particulate delivery vehicles, one must further avoid their excessive aggregation and consequent interference with material extrusion, such that occasional interruption of fiber continuity would be observed, with a resultant disruption in the intended pattern of the 3D printed layer. One major determinant of the likelihood of this undesired phenomenon is the diameter of the particulate delivery vehicles and/or their aggregates, which should ideally be at least one order of magnitude less than the inner diameter of the printing nozzle to avoid issues such as clogging during extrusion[10]. In the present study, particulate delivery vehicles of suitable size for extrusion-based 3D printing were synthesized, with an average particle diameter of 0.980 μm, compared to the needle inner diameter of 413 μm (22G). These desirably small particle sizes were enabled by the modification of two previously reported protocols, yielding an approximate 30-40 times reduction of average particle diameter compared to the original methods[21, 43].

In conclusion, 3D printed constructs fabricated at an elevated printing temperature (90 °C) were demonstrated to decrease the total amount of bioactive BMP-2 released, while physiologic (37 °C) or intermediate (60 °C) printing temperatures did not exhibit decreased bioactivity of released BMP-2 relative to that released from PLGA particles alone. Future biomaterial systems designed for delivery of this osteogenic growth factor should therefore be designed to allow printing temperatures less than 90 °C, through appropriate selection and modification of both bulk materials and intermediary carriers such as particulate delivery vehicles. This work highlights the capacity and considerations for preservation of BMP-2 bioactivity during extrusion-based 3D printing, towards the incorporation of bioactive growth factors in 3D printed scaffolds for bone tissue engineering applications.

Supplementary Material

Refer to Web version on PubMed Central for supplementary material.

Acknowledgements

This work was supported by the National Institutes of Health (Grant P41 EB023833). G.L.K. is supported by the Robert and Janice McNair Foundation MD/PhD Student Scholar Program. M.D. is supported by a Rubicon postdoctoral fellowship from the Dutch Research Council (NWO; Project No. 019.182EN.004). The authors gratefully acknowledge Anthony J. Melchiorri and Yu Seon Kim for their guidance on polymer synthesis, and Luis Diaz-Gomez for his input on 3D printing.

References

1. ASTMF2131: Standard test method for in vitro biological activity of recombinant human bone morphogenetic protein-2 (rh-BMP-2) using the W-20 mouse stromal cell line. 2012.
2. Bittner SM, Guo JL and Mikos AG. Spatiotemporal control of growth factors in three-dimensional printed scaffolds. Bioprinting 12:2018.
3. Bracaglia LG, Messina M, Vantucci C, Baker HB, Pandit A and Fisher JP. Controlled delivery of tissue inductive factors in a cardiovascular hybrid biomaterial scaffold. ACS Biomater. Sci. Eng 3:1350–1358, 2016. [PubMed: 33429693]
4. Busatto C, Pesoa J, Helbling I, Luna J and Estenoz D. Heterogeneous hydrolytic degradation of poly(lactic-co-glycolic acid) microspheres: mathematical modeling. J. Appl. Polym. Sci 134: 45464, 2017.
5. Caballero Aguilar LM, Silva SM and Moulton SE. Growth factor delivery: defining the next generation platforms for tissue engineering. J. Control. Release 306:40–58, 2019. [PubMed: 31150750]
6. Cai Z, Wan Y, Becker ML, Long YZ and Dean D. Poly(propylene fumarate)-based materials: synthesis, functionalization, properties, device fabrication and biomedical applications. Biomaterials 208:45–71, 2019. [PubMed: 30991217]
7. Clark A, Milbrandt TA, Hilt JZ and Puleo DA. Retention of insulin-like growth factor I bioactivity during the fabrication of sintered polymeric scaffolds. Biomed. Mater 9:025015, 2014. [PubMed: 24565886]
8. Coleman J and Lowman A. Biodegradable nanoparticles for protein delivery: analysis of preparation conditions on particle morphology and protein loading, activity and sustained release properties. J. Biomater. Sci. Polym. Ed 23:1129–1151, 2012. [PubMed: 21639993]
9. Comminal R, Serdeczny MP, Pedersen DB and Spangenberg J. Numerical modeling of the strand deposition flow in extrusion-based additive manufacturing. Addit. Manuf 20: 68–76, 2018.
10. Emmermacher J, Spura D, Cziommer J, Kilian D, Wollborn T, Fritsching U, Steingroewer J, Walther T, Gelinsky M and Lode A. Engineering considerations on extrusion-based bioprinting: interactions of material behavior, mechanical forces and cells in the printing needle. Biofabrication 12:025022, 2020. [PubMed: 32050179]
11. England JL and Haran G. Role of solvation effects in protein denaturation: from thermodynamics to single molecules and back. Annu. Rev. Phys. Chem 62:257–277, 2011. [PubMed: 21219136]
12. Farshid B, Lalwani G, Shir Mohammadi M, Simonsen J and Sitharaman B. Boron nitride nanotubes and nanoplatelets as reinforcing agents of polymeric matrices for bone tissue engineering. J. Biomed. Mater. Res. B Appl. Biomater 105:406–419, 2017. [PubMed: 26526153]
13. Fox N and Streinu I. “Redundant and critical noncovalent interactions in protein rigid cluster analysis.” In: Discrete and Topological Models in Molecular Biology, edited by Jonoska N and Saito M. Berlin, Heidelberg: Springer Berlin Heidelberg, 2014, pp. 167–196.
14. Freeman FE, Pitacco P, van Dommelen LHA, Nulty J, Browe DC, Shin J-Y, Alsberg E and Kelly DJ. 3D bioprinting spatiotemporally defined patterns of growth factors to tightly control tissue regeneration. Sci. Adv 6:eabb5093, 2020. [PubMed: 32851179]

15. Galarraga JH, Kwon MY and Burdick JA. 3D bioprinting via an in situ crosslinking technique towards engineering cartilage tissue. Sci. Rep 9: 19987, 2019. [PubMed: 31882612]
16. Holland TA, Tabata Y and Mikos AG. In vitro release of transforming growth factor-β1 from gelatin microparticles encapsulated in biodegradable, injectable oligo(poly(ethylene glycol) fumarate) hydrogels. J. Control. Release 91:299–313, 2003. [PubMed: 12932709]
17. Jain S, Fuoco T, Yassin MA, Mustafa K and Finne-Wistrand A. Printability and critical insight into polymer properties during direct-extrusion based 3D printing of medical grade polylactide and copolyesters. Biomacromolecules 21:388–396, 2020. [PubMed: 31566357]
18. Ji S, Dube K, Chesterman JP, Fung SL, Liaw CY, Kohn J and Guvendiren M. Polyester-based ink platform with tunable bioactivity for 3D printing of tissue engineering scaffolds. Biomater. Sci 7:560–570, 2019. [PubMed: 30534726]
19. Kasper FK, Tanahashi K, Fisher JP and Mikos AG. Synthesis of poly(propylene fumarate). Nat. Protoc 4:518–525, 2009. [PubMed: 19325548]
20. Kempen DH, Lu L, Hefferan TE, Creemers LB, Maran A, Classic KL, Dhert WJ and Yaszemski MJ. Retention of in vitro and in vivo BMP-2 bioactivities in sustained delivery vehicles for bone tissue engineering. Biomaterials 29:3245–3252, 2008. [PubMed: 18472153]
21. Kempen DH, Lu L, Kim C, Zhu X, Dhert WJ, Currier BL and Yaszemski MJ. Controlled drug release from a novel injectable biodegradable microsphere/scaffold composite based on poly(propylene fumarate). J. Biomed. Mater. Res. A 77:103–111, 2006. [PubMed: 16392139]
22. Kim K, Dean D, Wallace J, Breithaupt R, Mikos AG and Fisher JP. The influence of stereolithographic scaffold architecture and composition on osteogenic signal expression with rat bone marrow stromal cells. Biomaterials 32:3750–3763, 2011. [PubMed: 21396709]
23. Kim K, Lam J, Lu S, Spicer PP, Lueckgen A, Tabata Y, Wong ME, Jansen JA, Mikos AG and Kasper FK. Osteochondral tissue regeneration using a bilayered composite hydrogel with modulating dual growth factor release kinetics in a rabbit model. J. Control. Release 168:166–178, 2013. [PubMed: 23541928]
24. Kim S, Kang Y, Krueger CA, Sen M, Holcomb JB, Chen D, Wenke JC and Yang Y. Sequential delivery of BMP-2 and IGF-1 using a chitosan gel with gelatin microspheres enhances early osteoblastic differentiation. Acta Biomater. 8: 1768–1777, 2012. [PubMed: 22293583]
25. Koons GL, Diba M and Mikos AG. Materials design for bone-tissue engineering. Nat. Rev. Mater 5:584–603, 2020.
26. Koons GL and Mikos AG. Progress in three-dimensional printing with growth factors. J. Control. Release 295:50–59, 2019. [PubMed: 30579982]
27. Kyle S, Jessop ZM, Al-Sabah A and Whitaker IS. 'Printability' of candidate biomaterials for extrusion based 3D printing: state-of-the-art. Adv. Healthcare Mater 6:1700264, 2017.
28. Lakshmanan R, Kumaraswamy P, Krishnan UM and Sethuraman S. Engineering a growth factor embedded nanofiber matrix niche to promote vascularization for functional cardiac regeneration. Biomaterials 97:176–195, 2016. [PubMed: 27177129]
29. Lee C-U, Vandenbrande J, Goetz AE, Ganter MA, Storti DW and Boydston AJ. Room temperature extrusion 3D printing of polyether ether ketone using a stimuli-responsive binder. Addit. Manuf 28:430–438, 2019.
30. Lee J, Walker J, Natarajan S and Yi S. Prediction of geometric characteristics in polycaprolactone (PCL) scaffolds produced by extrusion-based additive manufacturing technique for tissue engineering. Rapid Prototyping J. 26:238–248, 2020.
31. Lee J, Walker J, Kang KS, Lee SH, Kim JY, Lee BK and Cho DW. Bone regeneration using a microstereolithography-produced customized poly(propylene fumarate)/diethyl fumarate photopolymer 3D scaffold incorporating BMP-2 loaded PLGA microspheres. Biomaterials 32:744–752, 2011. [PubMed: 20933279]
32. Luca L, Rougemont A-L, Waploth BH, Gurny R and Jordan O. The effects of carrier nature and pH on rhBMP-2-induced ectopic bone formation. J. Control. Release 147:38–44, 2010. [PubMed: 20600403]
33. Luo Y, Le Fer G, Dean D and Becker ML. 3D printing of poly(propylene fumarate) oligomers: evaluation of resin viscosity, printing characteristics and mechanical properties. Biomacromolecules 20:1699–1708, 2019. [PubMed: 30807696]

34. Mistry AS, Mikos AG and Jansen JA. Degradation and biocompatibility of a poly(propylene fumarate)-based/alumoxane nanocomposite for bone tissue engineering. J. Biomed. Mater. Res. A 83:940–953, 2007. [PubMed: 17580323]
35. Nyberg E, Holmes C, Witham T and Grayson WL. Growth factor-eluting technologies for bone tissue engineering. Drug Deliv. Transl. Res 6:184–194, 2016. [PubMed: 25967594]
36. Ohta H, Wakitani S, Tensho K, Horiuchi H, Wakabayashi S, Saito N, Nakamura Y, Nozaki K, Imai Y and Takaoka K. The effects of heat on the biological activity of recombinant human bone morphogenetic protein-2. J. Bone Miner. Metab 23:420–425, 2005. [PubMed: 16261447]
37. Olthof MGL, Kempen DHR, Herrick JL, Yaszemski MJ, Dhert WJA and Lu L. Effect of different sustained bone morphogenetic protein-2 release kinetics on bone formation in poly(propylene fumarate) scaffolds. J. Biomed. Mater. Res. B Appl. Biomater 106:477–487, 2018. [PubMed: 28186684]
38. Placone JK and Engler AJ. Recent advances in extrusion-based 3D printing for biomedical applications. Adv. Healthcare Mater. 7:e1701161, 2018.
39. Ramburrun P, Kumar P, Choonara YE, Bijukumar D, du Toit LC and Pillay V. A review of bioactive release from nerve conduits as a neurotherapeutic strategy for neuronal growth in peripheral nerve injury. Biomed. Res. Int 2014:132350, 2014. [PubMed: 25143934]
40. Roberts JJ, Naudiyal P, Jugé L, Bilston LE, Granville AM and Martens PJ. Tailoring stimuli responsiveness using dynamic covalent cross-linking of poly(vinyl alcohol)-heparin hydrogels for controlled cell and growth factor delivery. ACS Biomater. Sci. Eng 1:1267–1277, 2015. [PubMed: 33429674]
41. Seto SP, Miller T and Temenoff JS. Effect of selective heparin desulfation on preservation of bone morphogenetic protein-2 bioactivity after thermal stress. Bioconjugate Chem. 26:286–293, 2015.
42. Sevim K and Pan J. A mechanistic model for acidic drug release using microspheres made of PLGA 50:50. Molec. Pharm 13: 2729–2735, 2016. [PubMed: 27398973]
43. Shah SR, Henslee AM, Spicer PP, Yokota S, Petrichenko S, Allahabadi S, Bennett GN, Wong ME, Kasper FK and Mikos AG. Effects of antibiotic physicochemical properties on their release kinetics from biodegradable polymer microparticles. Pharm. Res 31:3379–3389, 2014. [PubMed: 24874603]
44. Smith BT, Bittner SM, Watson E, Smoak MM, Diaz-Gomez L, Molina ER, Kim YS, Hudgins CD, Melchiorri AJ, Scott DW, Grande-Allen KJ, Yoo JJ, Atala A, Fisher JP, and Mikos AGMulti-material dual gradient 3D printing for osteogenic differentiation and spatial segregation. Tissue Eng. Part A26:239–252, 2020. [PubMed: 31696784]
45. Suntornnond R, Tan EYS, An J and Chua CK. A highly printable and biocompatible hydrogel composite for direct printing of soft and perfusable vasculature-like structures. Sci. Rep 7:16902, 2017. [PubMed: 29203812]
46. Tarafder S, Koch A, Jun Y, Chou C, Awadallah MR and Lee CH. Micro-precise spatiotemporal delivery system embedded in 3D printing for complex tissue regeneration. Biofabrication 8:025003, 2016. [PubMed: 27108484]
47. Thibault RA, Baggett LS, Mikos AG, and Kasper FKOsteogenic differentiation of mesenchymal stem cells on pregenerated extracellular matrix scaffolds in the absence of osteogenic cell culture supplements. Tissue. Eng. Part A16:431–440, 2010. [PubMed: 19863274]
48. Timmer MD, Shin H, Horch RA, Ambrose CG and Mikos AG. In vitro cytotoxicity of injectable and biodegradable poly(propylene fumarate)-based networks: unreacted macromers, cross-linked networks, and degradation products. Biomacromolecules 4:1026–1033, 2003. [PubMed: 12857088]
49. Tousif Ayyub K, Moravkar K, Maniruzzaman M and Amin P. Effect of melt extrudability and melt binding efficiency of polyvinyl caprolactam polyvinyl acetate polyethylene glycol graft copolymer (Soluplus®) on release pattern of hydrophilic and high dose drugs. Mater. Sci. Eng. C Mater. Biol. Appl 99:563–574, 2019. [PubMed: 30889730]
50. Trachtenberg JE, Placone JK, Smith BT, Piard CM, Santoro M, Scott DW, Fisher JP and Mikos AG. Extrusion-based 3D printing of poly(propylene fumarate) in a full-factorial design. ACS Biomater. Sci. Eng 2:1771–1780, 2016. [PubMed: 33440475]

51. Turner BN, Strong R and Gold SA. A review of melt extrusion additive manufacturing processes: I. Process design and modeling. Rapid Prototyping J. 20: 192–204, 2014.
52. Wang MO, Etheridge JM, Thompson JA, Vorwald CE, Dean D and Fisher JP. Evaluation of the in vitro cytotoxicity of cross-linked biomaterials. Biomacromolecules 14:1321–1329, 2013. [PubMed: 23627804]
53. Wang MO, Piard CM, Melchiorri A, Dreher ML and Fisher JP. Evaluating changes in structure and cytotoxicity during in vitro degradation of three-dimensional printed scaffolds. Tissue Eng. Part A 21:1642–1653, 2015. [PubMed: 25627168]
54. Wei C, Solanki NG, Vasoya JM, Shah AV and Serajuddin ATM. Development of 3D printed tablets by fused deposition modeling using polyvinyl alcohol as polymeric matrix for rapid drug release. J. Pharm. Sci 109:1558–1572, 2020. [PubMed: 32004538]
55. Xiao J, Wang Y, Bellusci S and Li X. Pharmacological application of growth factors: basic and clinical. Biomed. Res. Int 2015:141794, 2015. [PubMed: 25685771]
56. Xu Y, Kim C-S, Saylor DM and Koo D. Polymer degradation and drug delivery in PLGA-based drug–polymer applications: a review of experiments and theories. J. Biomed. Mater. Res. B Appl. Biomater 105: 1692–1716, 2017. [PubMed: 27098357]
57. Xiao J, Wang Y, Bellusci S and Li X. Pharmacological application of growth factors: basic and clinical. Biomed. Res. Int 2015:141794, 2015. [PubMed: 25685771]
58. Yamakawa S and Hayashida K. Advances in surgical applications of growth factors for wound healing. Burns Trauma 7:10, 2019. [PubMed: 30993143]

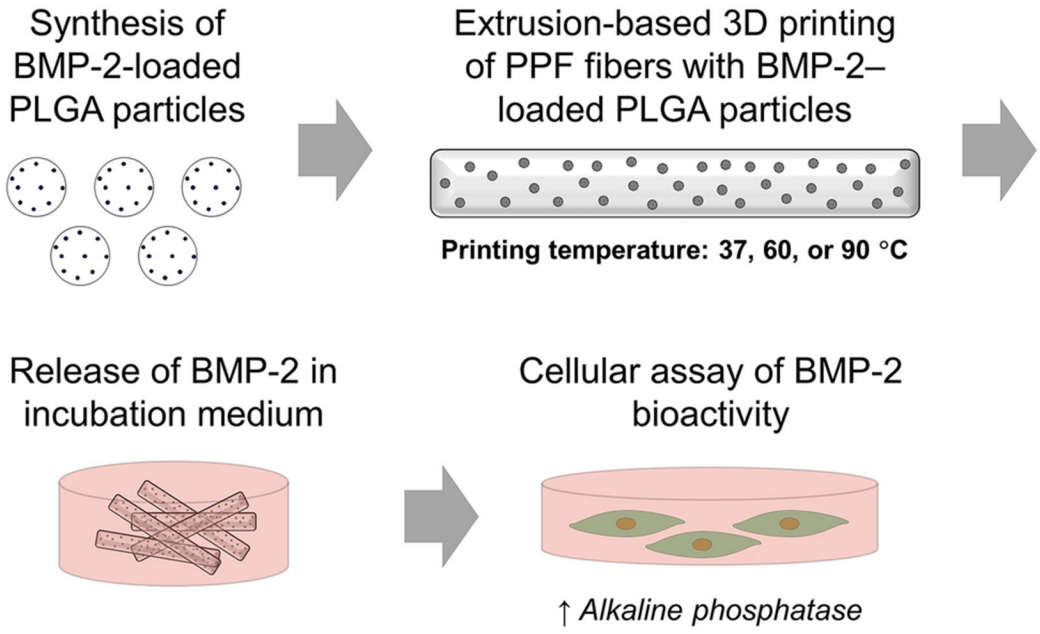

Figure 1. Overview of study design.

Schematic of fabrication of BMP-2–loaded 3D printed constructs, collection of released growth factor by incubation in aqueous medium, and exposure of collected release supernatants to W-20-17 cells for measurement of alkaline phosphatase activity.

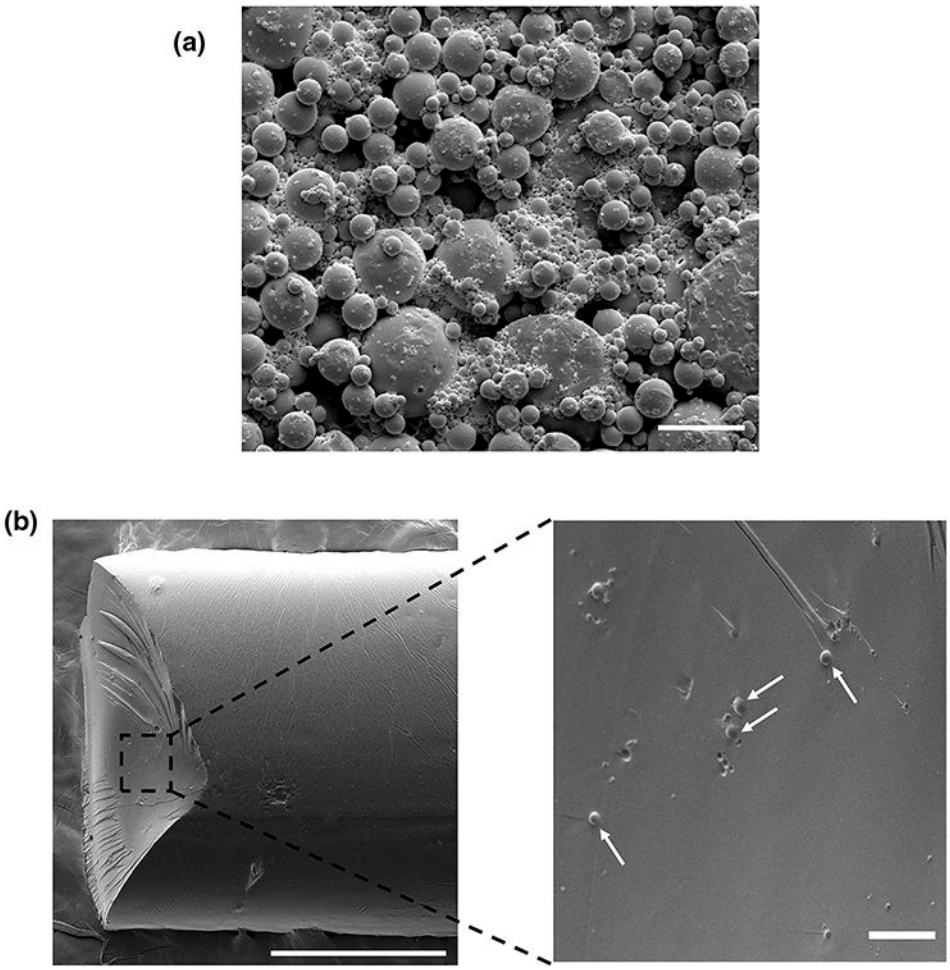

Figure 2. Morphology of delivery vehicles and 3D printed constructs.

A) Scanning electron microscopy (SEM) image of BMP-2–loaded PLGA particles. Scale bar = 10 μm. B) SEM image of extrusion 3D printed PPF-based fiber (left) and magnified cross-section view (right) with embedded PLGA particles indicated by white arrows. Scale bar = 500 μm (left) or 25 μm (right).

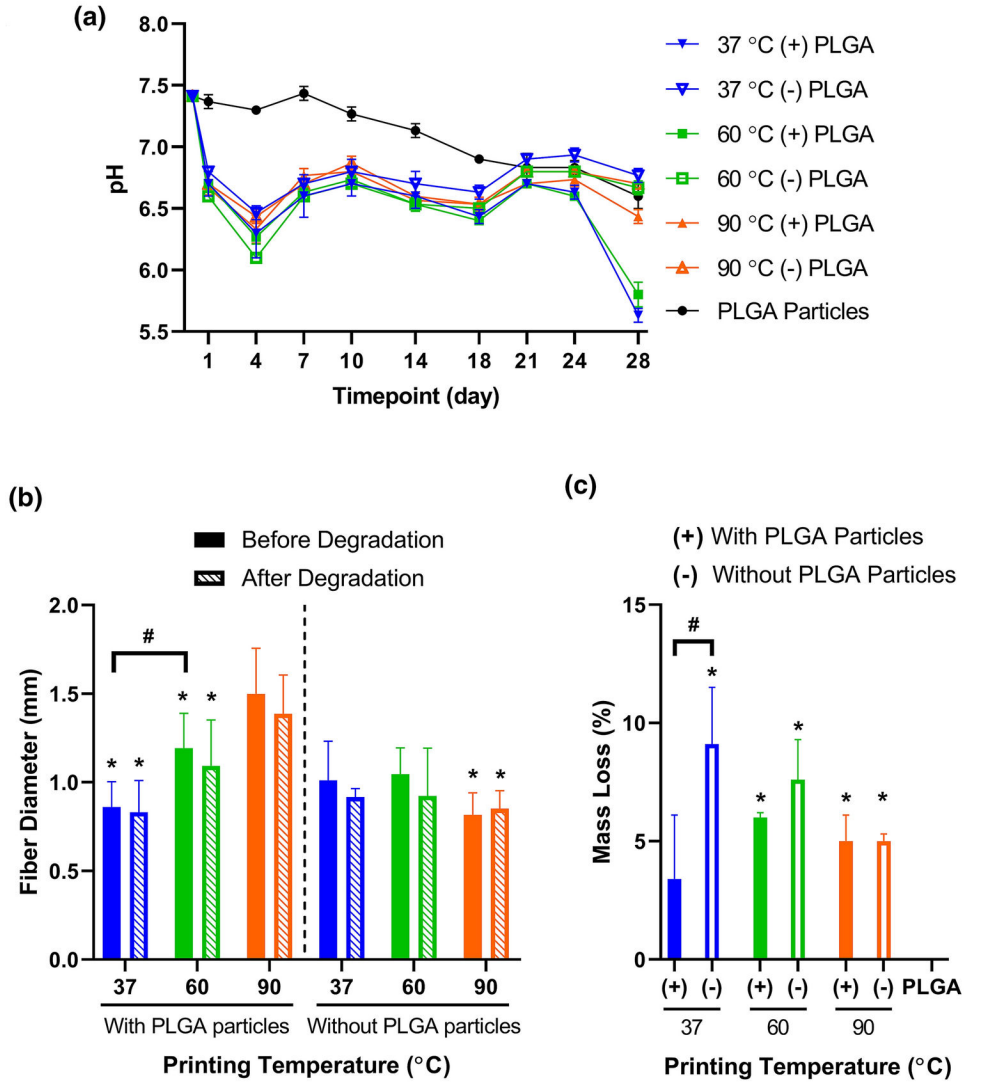

Figure 3. Characterization of degradation for 3D printed PPF-based fibers.

A) pH of degradation buffer during incubation with 3D printed PPF-based fibers or PLGA particles, with replacement of buffer at each measurement timepoint. Data are reported as mean ± standard deviation for $n = 3$ samples. Statistical comparisons can be found in Supplementary Table S1. B) Average diameters of ten randomly selected fibers from each material formulation and printing temperature, prior to or following 28 days of incubation in degradation buffer. * above a data bar indicates significant difference ($p < 0.05$) relative to the corresponding particle-containing 90 °C group, with pre-degradation groups compared to the pre-degradation particle-containing 90 °C group, and post-degradation groups compared to the post-degradation particle-containing 90 °C group; # above a line between data bars indicates significant difference ($p < 0.05$) between those groups. C) Percentage of sample mass loss during the 28-day degradation study. Data are reported as mean ± standard deviation for $n = 3$ samples. * above a data bar indicates significant difference ($p < 0.05$) relative to the PLGA particle-only control group; # above a line between data bars indicates

significant difference ($p < 0.05$) between those groups. (+) or (−) refers to printed fiber groups that either contain or do not contain PLGA particles, respectively.

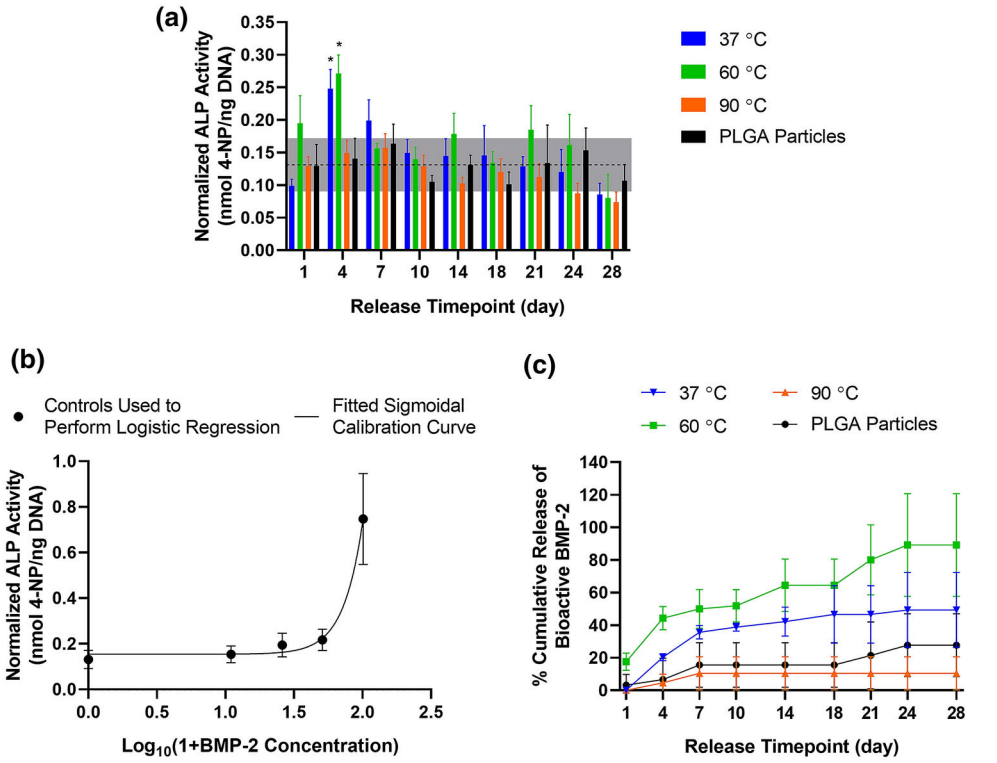

Figure 4. Cellular bioactivity assay of ALP upregulation.

A) ALP activity normalized by DNA content for W-20-17 cells. Horizontal dotted line indicates averaged value for control cells incubated in culture medium without added growth factor; grey box represents ± standard deviation of these controls cells' values. * denote significant upregulation ($p < 0.05$) from the averaged value for control cells as determined by unpaired t-tests. B) Calibration curve derived from four-point logistic regression which correlates normalized ALP activity of cells incubated with known concentrations of bioactive BMP-2 in ng/mL. C) Cumulative release profile of bioactive BMP-2 calculated from normalized ALP measurements for 3D printed constructs and PLGA delivery vehicles. Data are reported as mean ± standard deviation for $n = 3$-4 samples. Legends refer to printing temperature or non-printed PLGA particle control.

Table 1.

Ranges of printing parameters used for extrusion-based 3D printing.

Printing Temperature (° C)	Material Formulation	Range of Extrusion Pressures (bar)	Range of Printing Speeds (mm/s)
37	Without PLGA particles	7.0-7.0	0.1-0.1
	With unloaded PLGA particles	4.5-6.5	0.3-2.5
	With BMP-2–loaded PLGA particles	6.5-7.2	0.1-0.8
60	Without PLGA particles	1.0-2.0	0.4-1.0
	With unloaded PLGA particles	0.3-0.5	0.8-1.2
	With BMP-2–loaded PLGA particles	1.0-2.4	0.2-1.0
90	Without PLGA particles	0.2-0.2	2.0-2.5
	With unloaded PLGA particles	0.1-0.5	2.0-2.6
	With BMP-2–loaded PLGA particles	0.2-0.4	2.2-2.2